CHEMICAL AND STRUCTURAL EVOLUTION OF "METAMORPHIC VERMICULITE" IN METACLASTIC ROCKS OF THE BETIC CORDILLERA, MÁLAGA, SPAIN: A SYNTHESIS

María Dolores RUIZ CRUZ[§]

Departamento de Química Inorgánica, Cristalografía y Mineralogía, Universidad de Málaga,
Campus de Teatinos, E-29071 Málaga, Spain

José Miguel NIETO

Departamento de Geología, Facultad de Ciencias Experimentales, Universidad de Huelva, E-21071 Huelva, Spain

Abstract

Vermiculite-like minerals from a metamorphic sequence of the Betic Cordillera, near Málaga, southeastern Spain, were investigated in detail by X-ray diffraction, electron-microprobe analysis, and transmission-analytical electron microscopy. Our results reveal that the chlorite-to-biotite transformation is much more complex than previously assumed. In addition to mixed-layer minerals with a mica:chlorite ratio of 2:1 and 1:1, which had previously been identified, mixed-layer phases with very high and very low chlorite:vermiculite ratios have been identified, together with true vermiculite, as intermediate steps in the chlorite-to-biotite transformation. The observed sequence is: chlorite → random to ordered 1:2 mica–chlorite mixed-layer phases → regular 1:1 chlorite–vermiculite mixed-layer phases → Vrm-rich chlorite–vermiculite mixed-layer phases → vermiculite → biotite. This sequence includes a continuous increase of interlayer cation content, and is similar to that described in the smectite-to-illite transformation. The high Na content of most of these phases suggests that in the absence of K-feldspar, two parallel sites of reactants, chlorite + phengite and chlorite + albite, account for the formation of vermiculitic phases, and later, of biotite.

Keywords: mixed-layer minerals, metamorphic vermiculite, X-ray diffraction, electron-microprobe analysis, transmission electron microscopy, analytical electron microscopy, Betic Cordillera, Spain.

Sommaire

Nous avons étudié les minéraux de type vermiculite provenant d'une séquence métamorphique des Cordillères Bétiques près de Málaga, dans le sud-est de l'Espagne, au moyen de diffraction X, d'une microsonde électronique, et par microscopie électronique par transmission avec capacité analytique. Nos résultats montrent que la transformation de chlorite à biotite est beaucoup plus complexe qu'on ne l'avait soupçonné. En plus de minéraux à feuillets mixtes ayant un rapport mica:chlorite de 2:1 et 1:1, qui avaient déjà été signalés, nous trouvons des phases à feuillets mixtes ayant des rapports chlorite:vermiculite très élevés ou très faibles, ainsi que la vermiculite classique, comme stades intermédiaires dans la transformation de chlorite à biotite. La séquence observée est: chlorite → phases à feuillets mixtes ordonnées ou non ayant un rapport mica–chlorite de 1:2 → une intercalation régulière 1:1 de chlorite et vermiculite → phases à feuillets mixtes de chlorite et vermiculite enrichies en vermiculite → vermiculite → biotite. Cette séquence est marquée par une augmentation continue de la teneur en cations interfoliaires, et ressemble à celle qui a été décrite dans le cas de la transformation de smectite à illite, La teneur élevée en Na de la plupart de ces phases fait penser qu'en l'absence de feldspath potassique, deux sites de réactifs, chlorite + phengite et chlorite + albite, agissent en parallèle et rendent compte de la formation de phases vermiculitiques et, éventuellement, de la biotite.

(Traduit par la Rédaction)

Mots-clés: minéraux à feuillets mixtes, vermiculite métamorphique, diffraction X, microsonde électronique par transmission, microscopie électronique analytique, Cordillères Bétiques, Espagne.

[§] *E-mail address*: mdruiz@uma.es

INTRODUCTION

The onset of greenschist-facies metamorphism in many pelitic sequences from the outer margins of mountain belts is characterized by the mineral assemblage quartz + albite + phengite + chlorite ± K-feldspar, which defines the so-called "chlorite zone" of low-grade metamorphism. The appearance of biotite near the middle of the greenschist facies is an important temperature marker that indicates the beginning of the "biotite zone". Most reactions proposed for biotite formation at low-grade conditions consume chlorite, the most frequently cited (Yardley 1989, Miyashiro 1994) being 1) phengite + chlorite = biotite + muscovite + H_2O, and 2) K-feldspar + chlorite = biotite + muscovite + quartz + H_2O, which take place at about 400°C, at intermediate pressures.

On the other hand, the appearance of a yellow-to-brown phyllosilicate after chlorite just below the biotite zone has been known for many years. This phase was named "high-temperature vermiculite" or "metamorphic vermiculite" by Velde (1978) on the basis of its optical properties (high birefringence), chemical composition (similar to chlorite but containing some K and Ca), and thermal behavior (similar to that of vermiculite). The term "metamorphic vermiculite" includes, however, muscovite–chlorite intergrowths (Francescelli *et al*. 1986, Mellini *et al*. 1991), mixed-layered structures (Maresch *et al*. 1985, Ruiz Cruz 1999, 2001), and discrete single-phase vermiculite (or low-charge biotite) (Ruiz Cruz 1999). As a result, the more appropriate terms "vermiculitic phases" or "vermiculite" will be used in this work to designate phases showing optical and chemical similarities to "metamorphic vermiculite".

Here, we summarize results relative to vermiculitic phases from the Maláguide complex, in the Betic Cordillera of southeastern Spain, including new transmission electron microscope data that allow us to follow the complete structural evolution of these phases with increasing tectonic depth. We specifically focus on the chemical and structural characteristics of the vermiculite and the associated mineral assemblage in the Maláguide rocks of highest metamorphic grade, with the aim of determining their upper stability-limit.

BACKGROUND INFORMATION

Vermiculitic phases have been interpreted in cases as formed from chlorite during prograde metamorphism (*e.g*., Kerrick & Cotton 1971, Velde 1978, Maresch *et al*. 1985, Ruiz Cruz 1999, 2001, 2003), although there is also evidence of the formation of similar phases during weathering or retrograde processes affecting both chlorite and biotite (Johnson 1964, Brown 1967, Proust 1982, Proust *et al*. 1986).

Vermiculitic phases are common constituents of metaclastic pre-Ordovician to Carboniferous rocks of the Maláguide Paleozoic sequence of the Betic Cordillera, in southern Spain. Vermiculitic material commonly appears as a product of transformation of chlorite grains, at grain margins and along cleavage planes, the extent of transformation being variable from sample to sample and as a function of stratigraphic position. Thus, four main groups of rocks are encountered, corresponding to increasing metamorphic conditions:

I) Devonian to Carboniferous chlorite-rich samples, in which chlorite coexists with primary kaolinite-group minerals (dickite and nacrite). In these rocks, chlorite shows limited transformation to vermiculitic phases (Ruiz Cruz 2001).

II) Ordovician to Silurian chlorite-poor samples, occasionally containing chloritoid. Chlorite grains reveal a state of advanced transformation to vermiculitic phases (Ruiz Cruz 2001).

III) Ordovician chlorite-poor samples, containing garnet. Relics of unaltered chlorite are only rarely observed by optical microscopy.

IV) Older (Pre-Cambrian to Cambrian?) biotite-bearing samples, with common garnet and andalusite. In these samples, the grains of biotite and vermiculite cannot be differentiated by optical microscopy.

The older Paleozoic rocks have been included, in the Málaga area, with the Benamocarra Unit (see below).

OCCURRENCE AND PETROGRAPHY

The Betic Cordillera of SE Spain make up part of the peri-Mediterranean Alpine Orogenic system and crop out in a relatively continuous band of about 600 km in length (Fig. 1). This cordillera has been traditionally divided into a northern external domain, the Prebetic and the Subbetic zones, an intermediate domain, the flysch units from the Gulf of Cádiz area, and a southern internal domain, the Betic zone. The Alpine orogeny (Upper Cretaceous to Miocene) involved collision of the Internal and External zones. The collision was accompanied by intense structural deformation and metamorphism, which particularly affected the Internal zones. Structurally, the Internal zones include three main complexes: the Nevado–Filábride, the Alpujárride and the Maláguide, with decreasing metamorphic grade. Two successive Alpine events have been well characterized in the Nevado–Filábride complex: a high-pressure event (up to 20 kbar), corresponding to the eo-Alpine subduction process, and a meso-Alpine event with P–T conditions corresponding to the albite–epidote amphibolite facies (Puga *et al*. 2002). Although the Alpujárride complex shows important regional variations, it also records an Alpine low-temperature – high-pressure metamorphism (up to 11 kbar), overprinted by a high-temperature – low-pressure one (Azañón 1994, Azañón & Crespo Blanco 2000). The Maláguide complex is characterized, on the contrary, by conditions ranging from the diagenetic zone to the anchizone and
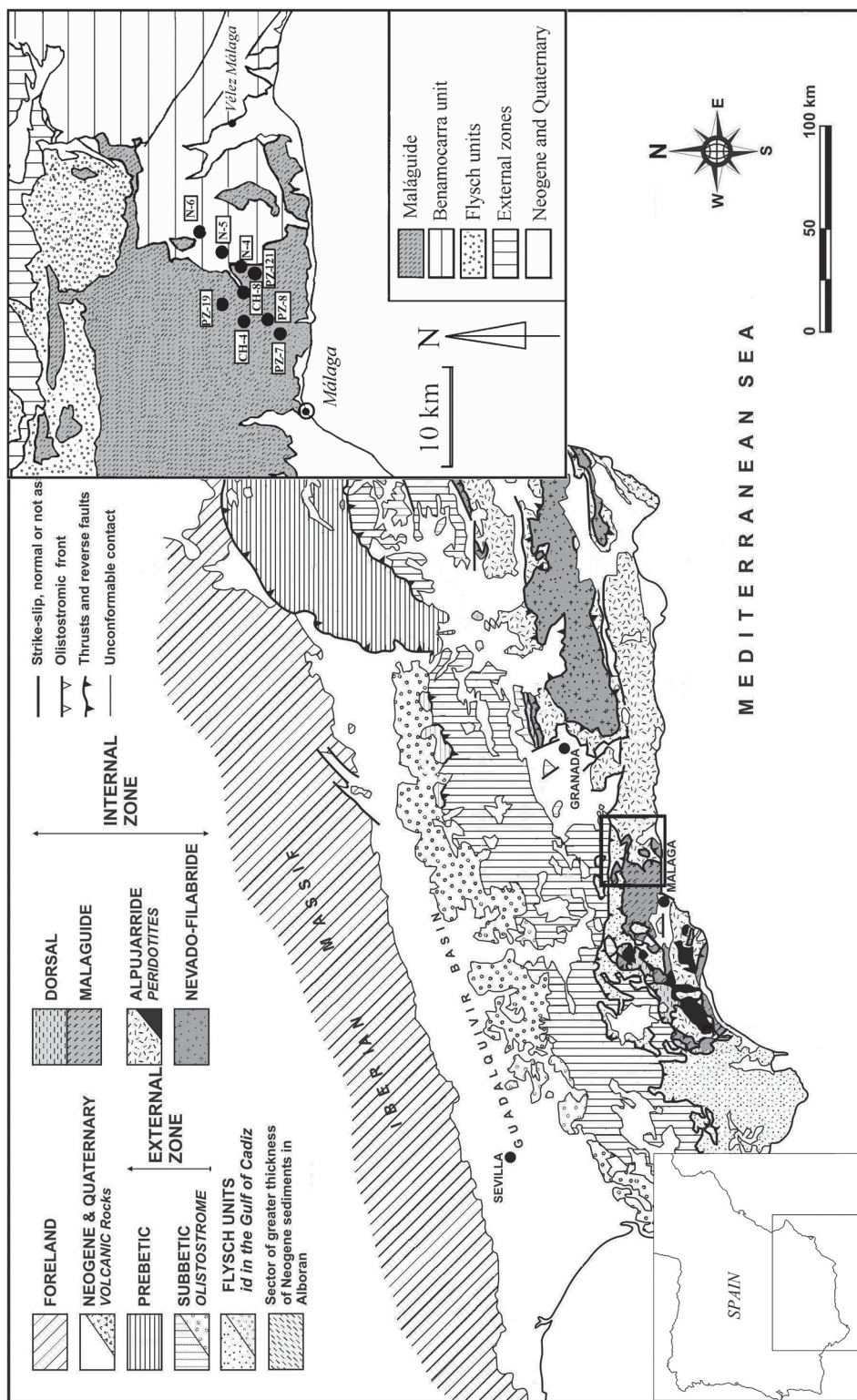
Fɪɢ. 1.   Tectonic sketch-map of the Betic Cordillera (modified from Sanz de Galdeano & Alfaro 2004). Inset: simplified map of the Málaga area showing the distribution of the Maláguide complex and the Benamocarra Unit, and the position of the samples cited in the work.

epizone (Ruiz Cruz & Rodríguez Jiménez 2002, Abad *et al.* 2003).

The main outcrop of the Maláguide complex selected for this study is located in the Málaga area (Fig. 1); the sequence includes Paleozoic (and probably Precambrian), Mesozoic and Tertiary sedimentary rocks. The Paleozoic unit is approximately 1.5 km thick, although the presence of several thinned tectonic slices suggests a greater initial thickness. This unit has been subdivided (Mäkel 1985) into: i) a greywacke-shale member (Carboniferous); ii) a limestone member (Devonian), and iii) a phyllite member (Ordovician–Silurian). The phyllite member structurally underlies early Paleozoic and Precambrian schists and mica schists, located between the Alpujárride and the Maláguide complexes, which have been grouped in an intermediate unit: Benamocarra. Although a considerable number of samples from the Málaga outcrop were studied and described previously, only samples cited in this paper are shown in Figure 1.

An optical microscopy study of shales, greywackes, phyllites, and schists led to the identification of three mafic phyllosilicates: chlorite, vermiculite and biotite. The chlorite shows a variable color, birefringence and optic sign, and variable degrees of transformation into vermiculite, according to stratigraphic position and sample grain-size. In Carboniferous shales, unaltered chlorite is the only mafic phyllosilicate. In coarse-grained rocks, grains of unaltered chlorite coexist with composite stacks of muscovite–chlorite, in which the chlorite areas show a variable transformation to a yellow-to-brown phyllosilicate with second-order birefringence and optical properties that agree with previous descriptions of "metamorphic vermiculite" (*e.g.*, Black 1975, Velde 1978, Nicot 1981) (Fig. 2A). In these samples, the mineral assemblages include quartz + albite + K-feldspar + carbonate + muscovite + chlorite (Table 1).

In Ordovician–Silurian phyllites, chlorite shows an advanced state of transformation to vermiculite (Fig. 2B). In some of these samples, the mineral assemblage includes paragonite, and locally, chloritoid. The deepest Ordovician (and probably older) schists are characterized by a significant decrease in chlorite, which is hardly discernible by optical microscopy, whereas vermiculite becomes the dominant mafic phyllosilicate (Fig. 2C). The mineral assemblage of these samples includes garnet, in some places unaltered, in others retrograded to Fe oxides. In these samples, vermiculite forms laths (0.05–0.2 mm) parallel to the S_1 schistosity. An evolution marked by increased grain-size and changing optical properties of the mafic grains (mainly darker color and pleochroism and higher birefringence) is observed in schists, which gradually leads to flakes of true biotite. In tectonically the deepest schists, the mineral assemblage includes andalusite. In these samples, vermiculite and biotite form large flakes (up to 1 mm long) parallel to S_1, intimately intergrown with muscovite (Fig. 2D). The parallel orientation of the metamorphic phases (vermiculite, white mica, and andalusite) as well as the boundaries between them, suggest textural equilibrium. Nevertheless, in some schists, two generations of vermiculite have been identified (Ruiz Cruz 2003), the first being parallel to the schistosity, and the second as pseudomorphs after garnet. In these schists, only the first generation of vermiculite is coeval with the other metamorphic phases.

EXPERIMENTAL TECHNIQUES

Samples were studied by X-ray diffraction (XRD) and electron-microprobe analysis (EMPA). In addition, samples representative of the various assemblages (Table 1) were studied by transmission and analytical electron microscopy (TEM–AEM).

X-ray diffraction

The XRD patterns were recorded at the Universidad de Málaga, using a Siemens D–5000 diffractometer with Cu*K*α radiation and a graphite monochromator, operated at 40 mA and 40 kV, with a step size of 0.01° 2θ and a step-count time of 1 s. Two size-fractions (<2 and 2–20 μm), separated by sedimentation, were systematically studied from each sample. Randomly oriented samples were analyzed to determine semiquantitatively the proportions of minerals. XRD patterns of oriented samples, obtained in the air-dried state (natural and Mg-exchanged), after ethylene glycol solvation and after heating at 550°C, allowed accurate identification of the phyllosilicates.

Electron-microprobe analyses

Polished and carbon-coated thin sections were studied with a Cameca SX–50 electron microprobe

TABLE 1. SUMMARY OF THE MINERAL ASSEMBLAGES
OF SELECTED SAMPLES

Type of samples	Asemblage of minerals	Samples	Lithology	Age
Chlorite-rich samples	Qtz + Ab ± Kfs ± Carb + Ms + Chl	PZ-7 PZ-8	Greywacke Shale	Carboniferous Carboniferous
Chlorite-poor samples	Qtz + Ab ± Kfs ± Carb + Ms ± Pg ± Cld ± Grt + "Vrm"	CH-4 PZ-121	Phyllite Phyllite	Devonian Ordovician-Silurian
		PZ-19	Phyllite	Ordovician-Silurian
		N-4 N-5	Schist Schist	Pre-Ordovician Pre-Ordovician
Biotite-bearing samples	Qtz + Ab ± Carb + Ms ± Pg ± Grt + And + "Vrm" + Bt	CH-8 N-6	Schist Schist	Pre-Ordovician Pre-Ordovician

Symbols: Qtz: quartz, Ab: albite, Kfs: K-feldspar, Carb: carbonates, Ms: muscovite, Pg: paragonite, Chl: chlorite, Vrm: vermiculite, Bt: biotite.
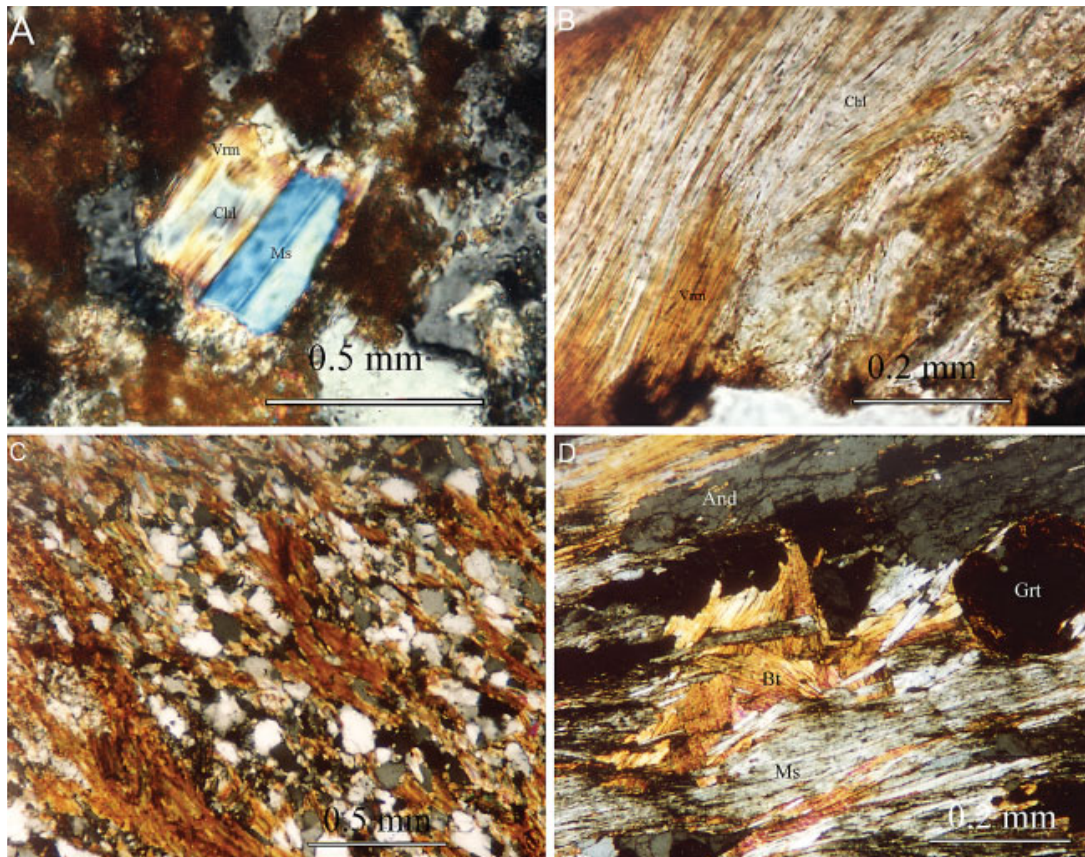
FIG. 2. Polarized-light micrographs showing: (A) A muscovite–chlorite stack in a Carboniferous greywacke (sample PZ–7). Chlorite shows an incipient transformation into vermiculitic phases. (B) Advanced transformation of a chlorite grain into vermiculitic phases (sample PZ–121). (C) Vermiculite flakes following the S_1 schistosity, in sample N–5. (D) Textural relations among muscovite, biotite (and vermiculite), andalusite and garnet in sample N–6. Garnet appears retrograded to Fe-oxide.

(EMPA) at the Universidad de Granada. Operating conditions were: accelerating voltage of 20 kV, beam current of 20 nA, and beam size of 5 μm. We used wollastonite (Si and Ca), synthetic Al_2O_3 (Al), orthoclase (K), albite (Na), synthetic Fe_2O_3 (Fe), periclase (Mg) and synthetic $MnTiO_3$ (Mn and Ti) as standards. The data were reduced using the X–PHI correction.

TEM–AEM study

For the TEM–AEM study, thin sections were prepared perpendicular to the S_1 schistosity. Copper grids were attached to selected areas, which were later separated from the glass backing. These areas were ion-thinned, carbon-coated and examined with a 200 kV JEOL 2000 FX microscope (Universidad Complutense, Madrid) and a 200 kV Philips CM–20 transmission electron microscope (Universidad de Granada), both fitted with a solid-state detector for energy-dispersion analysis

(EDX). Lattice-fringe images were obtained using 00*l* reflections and underfocus conditions corresponding to maximum contrast. Chemical analyses were obtained in the STEM mode for areas that were first characterized by electron diffraction and lattice-fringe imaging. Muscovite, albite, spessartine, forsterite and titanite were used as standards to calculate K-factors with the thin-film method of Lorimer & Cliff (1976).

RESULTS

XRD data

The XRD study permitted a first structural characterization of the mafic phases. Several groups of samples, defined by distinct assemblages of mafic phyllosilicates, correlate with increasing metamorphic grade (Table 1).

Figures 3 and 4 show the XRD patterns of some of these samples, in the range 0–30° (2θ). Reflections attributed to quartz, mica (10 Å) and chlorite or vermiculitic phases (14 and 7 Å) are clearly discernible. Vermiculitic phases are easily distinguishable from chlorite in the XRD patterns, on the basis of the 7 Å:14 Å ratio, which is very high in the case of chlorite and <1 where the sample contains vermiculitic phases.

Chlorite shows XRD patterns characteristic of a II*b* polytype, with a mean basal spacing d_{002} = 14.12 Å (Fig. 3A). Differences in Fe content do not greatly

affect the ratio of basal intensities; I_{001}/I_{002} ranges from 0.25 to 0.33 in the analyzed samples. The XRD patterns of samples containing mica–chlorite mixed-layers (Mi–Chl) are characterized by a set of 00*l* broad basal reflections with a mean spacing of 24.25 Å, although the first visible reflection is generally the 002 (Fig. 3B). The basal reflections do not change in position after ethylene glycol treatment, whereas a slight contraction accompanied by increased intensity of the 002 reflection is observed after heating at 550°C. Samples containing chlorite–vermiculite mixed-layers (Chl–Vrm) show XRD patterns clearly different from those shown by the Mi–Chl mixed-layers. They are characterized by a set of 00*l* reflections with mean spacing of 28.8 Å, corresponding to a regular 1:1 structure. Ethylene glycol solvation causes the expansion of the basal spacing to 29.0 Å, whereas heating at 550°C causes a contraction
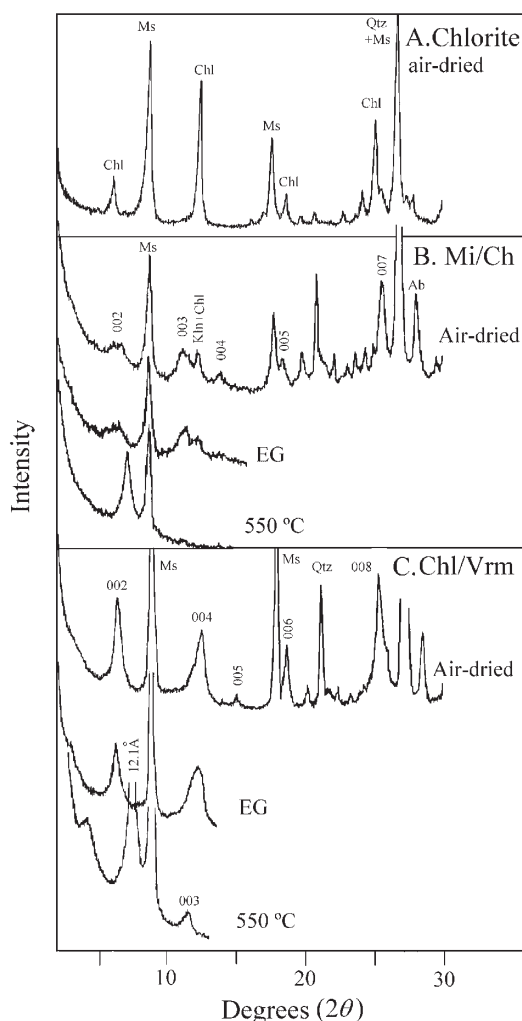

FIG. 3. X-ray-diffraction patterns of the <20 μm size-fractions, obtained from oriented samples. A. Chlorite-rich sample (PZ–8). B. Partially ordered Mi–Chl mixed-layer from sample PZ–7. C. Regular 1:1 Chl–Vrm mixed-layer from sample PZ–19. In B and C, the mixed-layer reflections have been labeled.
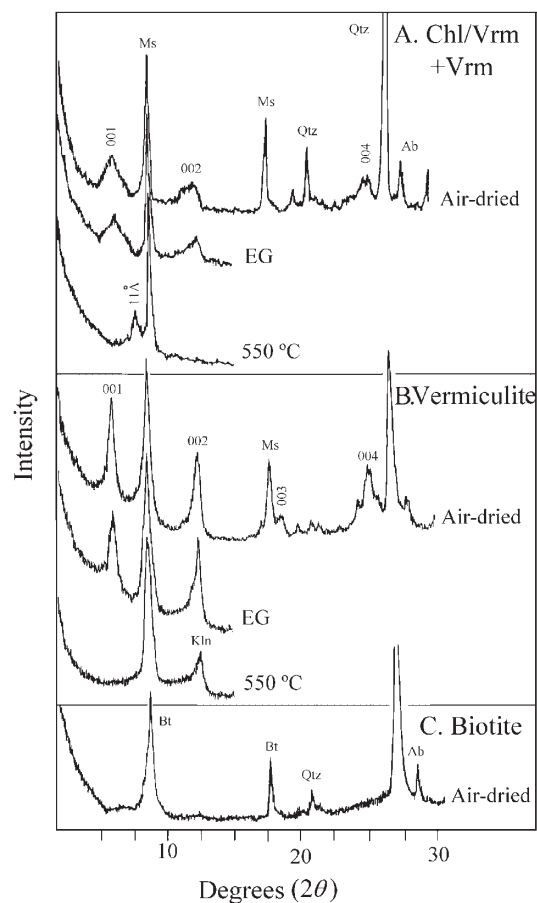

FIG. 4. X-ray-diffraction patterns of the <20 μm size-fractions, obtained from oriented samples. A. Vrm-rich Chl–Vrm mixed-layers from sample N–5. B. Vermiculite from sample Ch–8. C. Biotite from sample N–6.

to 24.12 Å (Fig. 3C). Chl–Vrm mixed-layers in some samples show a larger contraction after heating at 550°C, reflecting a higher content of vermiculite in the interstratified structure (Fig. 4A).

Samples containing discrete vermiculite are characterized by a main reflection at about 14 Å in samples saturated with Mg. Ethylene glycol solvation causes a very slight shift of the 14 Å reflection, and heating causes the gradual contraction of the basal reflection to 10 Å (Fig. 4B). The XRD patterns of samples containing biotite as the main mafic phyllosilicate are characterized by a basal reflection with a mean spacing of 10 Å. Nevertheless, the 10 Å reflection commonly shows a weak shoulder toward the high-angle region, suggesting the presence of some vermiculite-like layers in the biotite structure. The presence of a 7 Å reflection in the air-dried pattern of the Mi–Chl-bearing samples (Fig. 3B) indicates the presence of both chlorite and a primary kaolinite-group mineral (dickite), whereas the presence of a 7 Å reflection after heating at 550°C in some samples (*e.g.*, Fig. 4B), indicates the presence of kaolinite.

Electron-microprobe data

Results of EMPA analyses of these phyllosilicates have been previously published (Ruiz Cruz 1999, 2001, 2003). We report here the new data for samples N–4, N–5 and N–6, which are used for an estimation of the P–T conditions of metamorphism. Nevertheless, previously published data also have been used in the figures.

The composition of the white mica was recalculated on the basis of 11 atoms of oxygen and assuming all iron to be ferrous (Table 2). The muscovite is homogeneous within each sample as well as among the three samples studied. The Si content varies between 3.08 and 3.17 *apfu* (atoms per formula unit), whereas the total interlayer charge ranges from 0.86 to 0.97, the Na content being on the order of 0.1 *apfu*.

The composition of the garnet also is similar in the three samples; it is almandine-rich (Table 2). The Ca content varies between 0.32 and 0.65 *apfu*. The Mn content shows the most significant differences among the three samples, being on the order of 0.7 *apfu* in samples N–4 and N–6 and <0.10 *apfu* in sample N–5.

The composition of chlorite was recalculated on the basis of 14 atoms of oxygen, assuming all iron to

TABLE 2. SELECTED RESULTS OF EMPA ANALYSES OF MINERALS FROM SAMPLES N-4, N-5 AND N-6

	Ms			Chl		Vermiculitic phases					Low-charge biotite			Garnet			Andalusite
	N-4	N-5	N-6	N-4	N-5	N-4			N-5			N-6			N-4	N-5	N-6	N-5
SiO$_2$ wt%	47.82	46.68	46.44	26.50	26.15	27.24	29.14	32.03	26.10	29.55	38.07	34.86	36.23	37.26	37.02	37.15	36.90	39.66
Al$_2$O$_3$	33.86	36.57	35.80	21.13	21.02	19.93	17.95	20.01	18.74	20.31	21.47	19.55	19.71	20.37	20.90	21.13	20.83	59.74
TiO$_2$	0.26	0.34	0.37	0.30	0.05	0.05	0.12	0.17	4.93	0.14	0.59	1.69	2.35	2.19	0.08	0.12	0.13	0.04
FeO	1.85	0.91	0.86	26.49	27.19	25.80	27.63	22.85	25.62	28.44	23.61	17.00	16.42	15.64	26.73	31.69	24.23	0.28
MnO	0.02	0.00	0.00	0.34	0.33	0.21	0.19	0.13	0.11	0.14	0.07	0.16	0.16	0.16	10.28	0.35	10.08	0.05
MgO	1.25	0.59	0.59	11.90	11.76	8.93	8.50	7.43	8.63	7.66	5.25	6.35	7.35	8.03	1.39	1.87	0.83	0.05
CaO	0.06	0.01	0.01	0.19	0.13	0.61	0.69	0.57	0.18	0.43	0.60	0.40	0.44	0.14	3.68	7.57	6.00	0.00
Na$_2$O	0.58	0.75	0.68	0.03	0.04	0.07	0.13	0.13	0.03	0.09	0.16	0.21	0.15	0.10	0.00	0.03	0.03	0.03
K$_2$O	9.46	9.93	9.55	0.18	0.12	0.50	0.56	0.49	0.95	0.99	2.18	5.69	6.52	7.70	0.01	0.01	0.00	0.02
Total	95.15	95.81	95.81	87.04	86.83	86.83	84.98	83.84	85.34	87.76	87.00	85.65	89.33	91.59	100.10	99.96	99.03	99.88
Si *apfu*	3.16	3.08	3.09	2.82	2.81	3.11	3.20	3.43	2.86	3.15	3.44	2.86	2.85	2.84	3.00	2.98	3.01	1.07
^{IV}Al	0.84	0.92	0.91	1.18	1.19	0.89	0.80	0.57	1.14	0.85	0.56	1.14	1.15	1.16	0.00	0.02	0.00	0.00
^{VI}Al	1.80	1.92	1.89	1.47	1.47	1.53	1.52	1.95	1.28	1.70	2.07	0.75	0.67	0.67	1.99	1.98	2.00	1.90
Ti	0.01	0.02	0.02	0.02	0.00	0.00	0.01	0.01	0.41	0.01	0.05	0.10	0.14	0.13	0.00	0.01	0.00	0.00
Fe	0.10	0.05	0.05	2.36	2.44	2.47	2.54	2.05	2.34	2.53	2.05	1.10	1.08	1.00	1.81	2.12	1.65	0.01
Mn	0.01	0.00	0.00	0.03	0.03	0.02	0.02	0.01	0.01	0.01	0.00	0.01	0.01	0.01	0.71	0.02	0.70	0.00
Mg	0.12	0.06	0.06	1.89	1.89	1.52	1.39	1.19	1.41	1.22	0.81	0.77	0.86	0.91	0.17	0.22	0.10	0.00
Σoct.	2.04	2.05	2.02	5.77	5.83	5.54	5.48	5.21	5.45	5.47	4.98	2.73	2.76	2.72				
Ca	0.00	0.00	0.00	0.02	0.02	0.07	0.08	0.07	0.02	0.05	0.07	0.03	0.04	0.01	0.32	0.65	0.52	0.00
Na	0.07	0.10	0.09	0.00	0.01	0.02	0.03	0.03	0.01	0.02	0.03	0.03	0.02	0.01	0.00	0.00	0.00	0.00
K	0.80	0.84	0.81	0.02	0.02	0.07	0.08	0.07	0.13	0.14	0.29	0.59	0.65	0.75	0.00	0.00	0.00	0.00
Σint.	0.87	0.94	0.90	0.04	0.05	0.16	0.19	0.17	0.16	0.21	0.39	0.65	0.71	0.77				
O	11	11	11	14	14	14	14	14	14	14	14	11	11	11	12	12	12	5

be ferrous. Compositions of chlorite are homogeneous within individual samples, spanning, in the upper samples, from the clinochlore to the chamosite field (Fig. 5). The composition is more homogeneous in the deepest samples (Table 2), with Si content on the order of 2.80 *apfu* and the Fe/(Fe + Mg) value close to 0.55 (magnesian chamosite).

Vermiculitic phases have a more variable composition than chlorite. The transition from chloritic to vermiculitic areas within a grain or sample is characterized by an increase in SiO_2 content, a decrease in both Fe and Mg contents, and the presence of variable amounts of Ca, Na and K. This trend is also observed if samples from different metamorphic grade are plotted together (Fig. 6). These plots show that the amount of FeO shows a negative correlation with SiO_2, whereas that of MgO shows a poor negative correlation with SiO_2. Only the sum CaO + Na_2O + K_2O correlates positively with SiO_2. This correlation is less evident if CaO, Na_2O and K_2O are plotted separately against SiO_2, which indicates a range of CaO:Na_2O:K_2O proportions in the populations of samples. This general trend is also observed if we compare the compositional range of vermiculitic phases in samples N–4, N–5 and N–6 (Table 2): the mean SiO_2 content increases from samples N–4 and N–5 to sample N–6, and the mean K_2O increases in parallel. Based on chemical differences, which suggest an evolution from chlorite toward biotite, structural formulae have been calculated for 14 atoms of oxygen in samples N–4 and N–5 and for 11 atoms of oxygen in sample N–6. These formulae, which permit the comparison with true chlorite (in the case of samples N–4 and N–5) and with true biotite (in sample N–6) are, however, unrealistic. In fact, the interlayer charge calculated indicates that
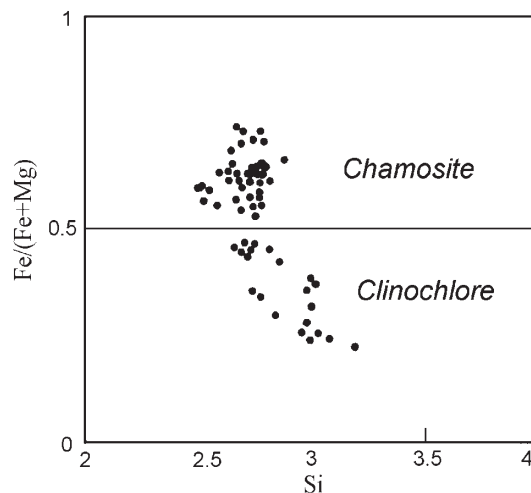
most compositions from samples N–4 and N–5 do not correspond to chlorite. Similarly, the interlayer charge in grains from sample N–6 (<0.80) indicates that most of these grains are not true biotite.

Fig. 5. Results of EMPA analyses of chlorite in a Fe/(Fe + Mg) *versus* Si diagram.
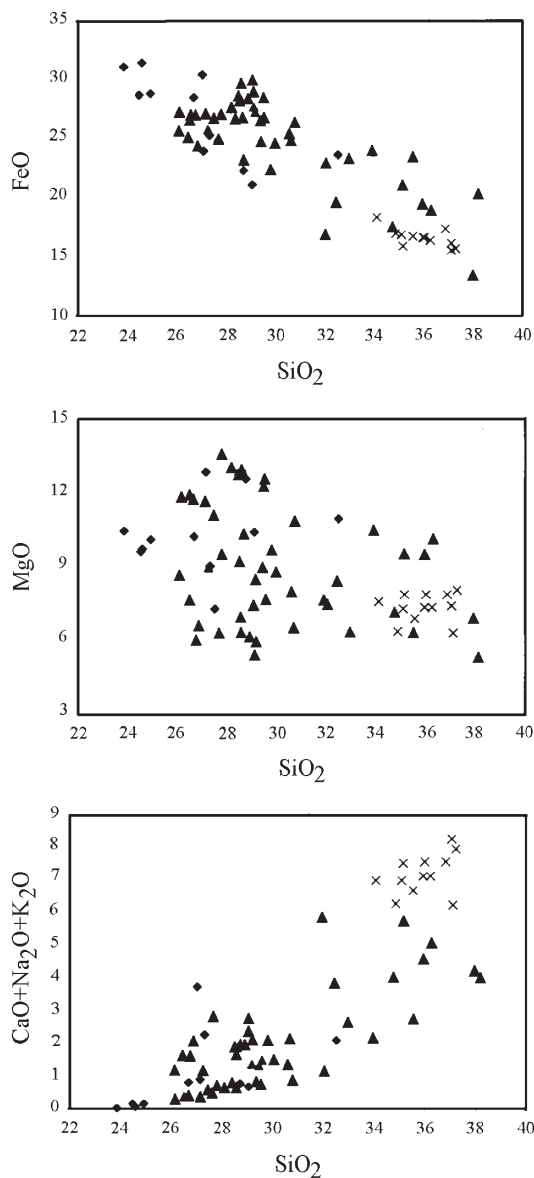

Fig. 6. Plots of significant chemical data relevant to vermiculitic phases. Oxide values are in wt.%. Full diamonds: compositions of chlorite-rich samples. Full triangles: compositions from chlorite-poor samples. Crosses: compositions from biotite-bearing samples.

TEM–AEM study

The TEM–AEM study of samples containing the above assemblages has led to the identification of a complete sequence of structures intermediate between chlorite and biotite (Figs. 7, 8). The AEM data from these samples have been previously published (Ruiz Cruz 1999, 2001, 2003). We present only chemical data corresponding to the images of Figures 7 and 8 (Table 3). Data in this table show the formulae of discrete phases. The formulae of the mixed-layer phases have not been calculated. We include, however, the atomic %, which permit comparisons among the several phases.

In chlorite-rich samples, chlorite grains are characterized by sequences of layers with a 14 Å periodicity, with local changes in layer thickness, from 14 to 10 Å and layer terminations (Fig. 7A). Disordered polytypes of chlorite, as well as one-, two-, and three-layer ordered polytypes, have been identified. The AEM data obtained from these packets (Table 3, anal. 1) show, as expected, a low $(Ca + Na + K)$ content, and are consistent with the compositions deduced from electron-microprobe analyses. The vermiculitic phase coexisting with chlorite in these samples varies from random to ordered Mi–Chl mixed-layer, characterized by the presence of dominant 38 Å periodicity in the lattice-fringe images (Fig. 7B). The selected-area electron-diffraction (SAED) patterns
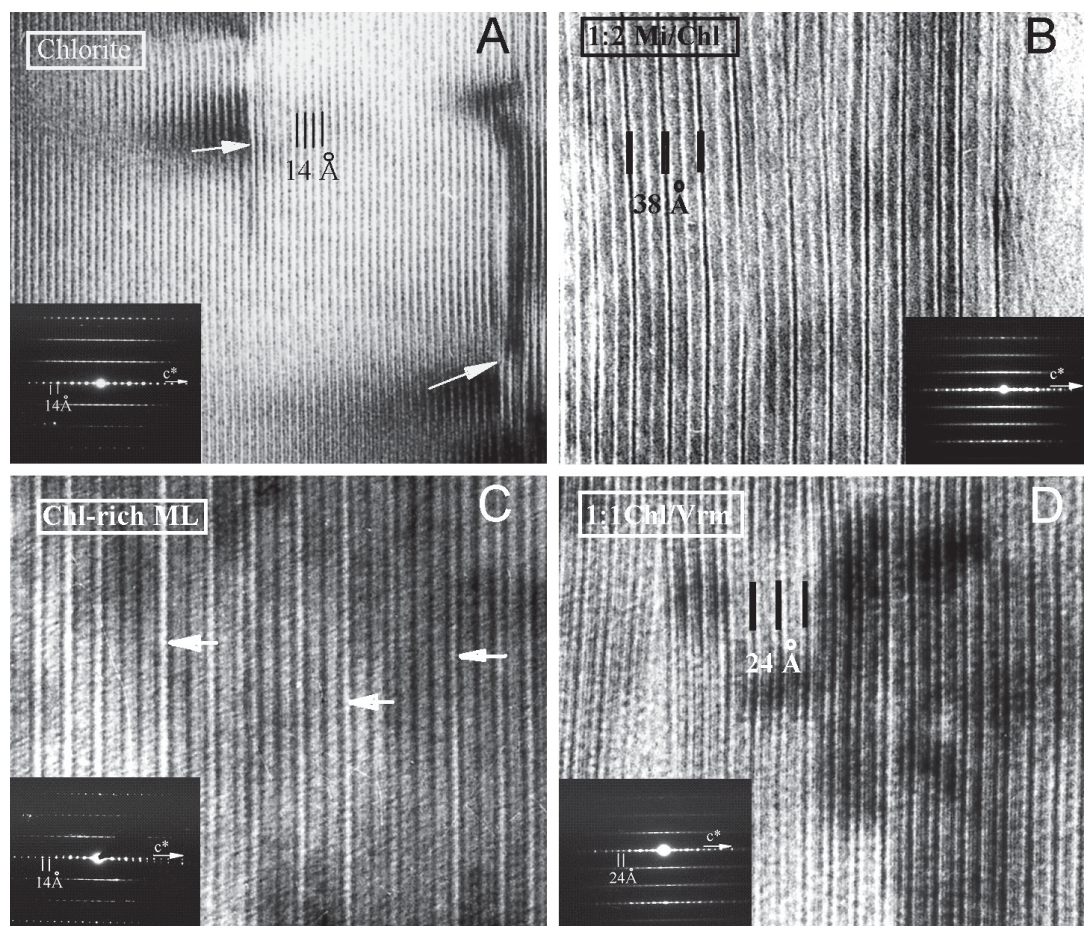

FIG. 7.   Lattice-fringe images of chlorite and vermiculitic phases at increasing metamorphic grade. A: Chlorite images show a 14 Å periodicity. Arrows indicate layer terminations. The SAED patterns reveals a well-ordered polytype (sample PZ–7). B. Sequences of regular 1:2 mica–chlorite (Mi–Chl) mixed-layers, which coexist with chlorite from image A. The SAED pattern shows irrational reflections. (sample PZ–7). C. Chlorite-rich mica–chlorite mixed-layers (ML) from sample PZ–19. Arrows indicate the 10 Å layers interstratified in the chlorite structure. The SAED pattern shows, however, a regular 14 Å periodicity. D. Regular 1:1 chlorite–vermiculite mixed-layer sequences in sample PZ–19. The SAED pattern shows a regular 24 Å periodicity.
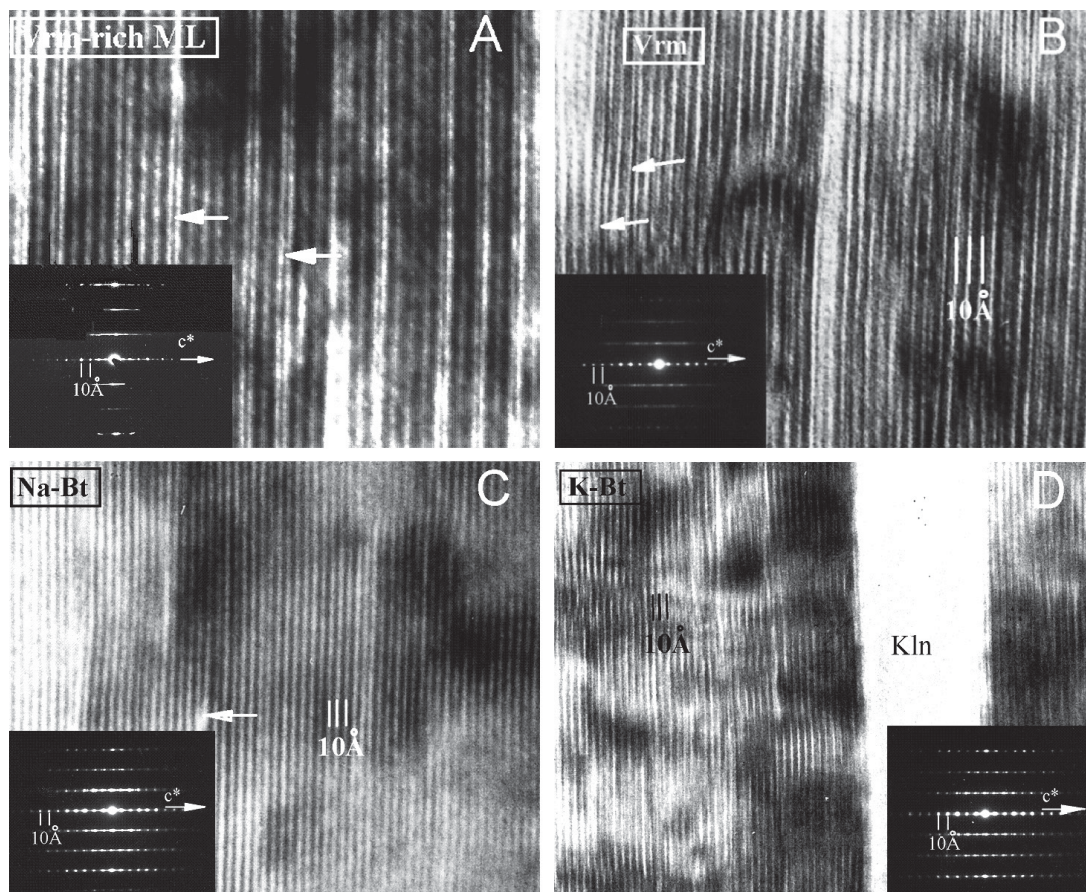
FIG. 8. Lattice-fringe images of vermiculitic phases, at increasing metamorphic grade. A. Vermiculite-rich chlorite–vermiculite mixed-layers (ML) from sample N–4. Arrows indicate the 14 Å fringes interstratified in the vermiculite structure. The SAED pattern shows 00*l* reflections with 10 Å periodicity. B. Vermiculite packets from sample N–5 containing scarce 14 Å fringes (white arrows). The SAED pattern reveals a regular 10 Å periodicity. The 0*kl* reflection rows indicate a disordered polytype. C. Image of sodian biotite with regular 10 Å periodicity (sample N–6). These packets show frequent slightly damaged areas (arrow). D. Image of a biotite packet, partially transformed into kaolinite (Kln) (sample N–6). In both K- and Na-rich packets, the SAED patterns suggest the presence of a three-layer polytype.

show generally irrational reflections (*i.e.,* they do not obey the Bragg law). The AEM data obtained from these packets (*e.g.*, Table 3, anal. 2) indicate a di,trioctahedral composition (Ruiz Cruz 2001), showing a wide range in (Ca + Na + K) content, and a higher Si content than that of chlorite. The interlayer cations include Ca, Na and K.

In chlorite-poor samples, the chlorite grains show lattice-fringe images in which the fringes with dominant 14 Å periodicity include abundant interstratified 10 Å layers (Fig. 7C). The SAED patterns reveal, however, only the 14 Å periodicity. Analysis of these packets (Table 3, anal. 3, 4) reveals low but constant amounts of Ca, Na and K. The vermiculitic phases identified in chlorite-poor samples at increasing metamorphic grade include regular 1:1 Chl–Vrm mixed-layers (Fig. 7D), vermiculite-rich randomly ordered Chl–Vrm mixed-layers (Fig. 8A) and vermiculite (Fig. 8B). The packets consisting of 1:1 Chl–Vrm mixed layers show generally high regularity, with sequences of 24 Å, reaching up to 1000 Å in thickness. The SAED patterns confirm the structural order (Fig. 7D). The AEM data obtained from these packets (Table 3, anal. 5) indicate an increase in Si content relative to chlorite and the 1:2 Mi–Chl mixed-layers, and variable Ca:Na:K proportions.

In samples N–4 and N–5 chlorite with a high density of 10 Å layers coexists with vermiculite, characterized by a 10 Å periodicity in the SAED patterns. The lattice-

fringe images reveal, however, that vermiculitic packets contain in cases numerous 14 Å fringes, randomly distributed (Fig. 8A). At higher metamorphic grade, the vermiculite packets show a higher structural regularity (Fig. 8B), although the AEM data are very similar (Table 3, anal. 6, 7). The vermiculite packets are either unaltered or with a variable degree of transformation to a dioctahedral phase identified as kaolinite from the AEM data and the SAED patterns. Kaolinite is interpreted as having formed during the retrograde stage.

Finally, in biotite-bearing samples, two types of packets have been identified: Na-rich and K-rich packets. The Na-rich packets shows regular 10 Å periodicity (Fig. 8C). The Si content is on the order of 3.30 *apfu*, and Fe/(Fe + Mg) ranges between 0.65 and 0.85 (*i.e.*, sodian annite). The interlayer charge ranges from 0.60 to 0.82 (Table 3, anal. 8). These packets can be interpreted as low-charge, hydrated Na-rich biotite, which behaves in XRD as vermiculite (Ruiz Cruz 2004). Similar material has been described by Dempster & Jackson (1996) and Ruiz Cruz & Novak (2003); it is clearly different from the sodium analogue of phlogopite described by Schreyer *et al.* (1980) and Spear *et al.* (1981). Biotite shows lattice-fringe images characterized by a mottled aspect (Fig. 8D). These packets show a Si content ranging from 2.78 to 3.03 *apfu*, an interlayer charge ranging from 0.86 to 0.99, and a Fe/(Fe + Mg) value near 0.50 (Table 3, anal. 9). As in the case of vermiculite packets, biotite packets appear commonly retrograded to kaolinite.

DISCUSSION

Origin of the vermiculitic phases

An important point concerns to the processes that lead to the formation of vermiculitic phases throughout the Paleozoic sequence. The mineral evolution observed at increasing tectonic depth can be simplified as follows: Chl → 1:2 Mi–Chl mixed-layers (step 1) → 1:1 Chl–Vrm mixed-layers (step 2) → Vrm (step 3) → Bt (step 4).

This sequence could be the result of either a prograde evolution of chlorite or the sum of a set of prograde and retrograde (or weathering) processes that affected to both chlorite and biotite.

There is microscopic evidence indicating that steps 1 and 2 (formation of 1:2 Mi–Chl and 1:1 Chl–Vrm mixed-layers) represent the transformation of chlorite (Figs. 2A, B). Indeed, temperatures estimated for these assemblages are in most cases clearly <400°C (see below), and the possibility of the previous presence of metamorphic biotite can be discarded.

The weathering of chlorite to Chl–Vrm mixed-layers (step 2) and vermiculite (step 3) is a well-documented process, observed experimentally (Ross 1975, Ross & Kodama 1976) and in natural environments (*e.g.* Johnson 1964, Ross *et al.* 1982, Proust *et al.* 1986,

Murakami *et al.* 1996, Banfield & Murakami 1998). During weathering, the vermiculitic phases formed at the expense of chlorite and contain, as expected, a very low content of K and a lack of Na and Ca (see Murakami *et al.* 1996). This is not the case for the vermiculitic phases described here, which contain appreciable amounts of (K + Na + Ca), suggesting that weathering (or retrogression) were not the processes leading to vermiculitic phases.

On the other hand, it is very difficult (probably impossible) to interpret the formation of Mi–Chl mixed-layers (step 1) as formed from weathering (or retrogression) of chlorite. Indeed, these types of interstratified structures have been never described as weathering (or retrogression) products of chlorite. On the contrary, Mi–Chl mixed-layers have been interpreted as prograde phases formed either from a smectitic precursor, during diagenesis and the first stages of the metamorphism (*e.g.*, Lee & Peacor 1985, Ahn *et al.* 1988), or from chlorite, during a higher-grade episode of metamorphism (Maresch *et al.* 1985).

From these data, it seems clear that steps 1 and 2, which show a progressive chemical evolution (Fig. 6), represent two stages of the same prograde reaction. There is no microscopic evidence about the precursor phase for vermiculite (step 3), such as that shown in Figure 2C. In addition, the metamorphic temperature attained for these samples is >400°C (see below), suggesting that vermiculite could represent either prograde evolution of the Chl–Vrm mixed-layers or retrogression of biotite. Indeed, weathering of biotite to

TABLE 3. SELECTED AEM DATA FOR CHLORITE AND
VERMICULITIC PHASES

Samples:	Chl-rich		Chl-poor					Bt-bearing	
	1	2	3	4	5	6	7	8	9
	Chl	ML	Chl	Chl	ML	Vrm	Vrm	Na-Bt	Bt
Figure no.	7A	7B	7C	N.S.	7D	8A	8B	8C	8D
Si (at.%)	28.75	34.43	30.73	32.16	35.80	36.60	38.05	44.69	38.97
Al	27.64	33.84	25.69	26.37	31.42	26.06	25.80	21.67	23.63
Ti	0.02	0.04	0.10	0.35	0.00	0.97	0.87	0.13	1.31
Fe	27.94	23.83	24.13	21.36	14.68	13.94	14.17	19.71	11.37
Mg	15.07	15.10	16.19	16.97	10.93	14.19	13.20	3.98	12.81
Ca	0.02	0.53	1.08	1.37	1.00	1.26	1.07	2.06	0.34
Na	0.20	2.62	1.29	0.16	1.40	2.24	3.88	6.20	2.13
K	0.40	3.56	0.81	1.27	4.77	4.74	4.57	1.57	9.45
Si (*apfu*)	2.83		3.02	3.11		2.74	2.83	3.24	2.93
^{IV}Al	1.17		0.98	0.89		1.26	1.17	0.76	1.07
^{VI}Al	1.55		1.54	1.66		0.69	0.75	0.81	0.71
Ti	0.00		0.01	0.03		0.07	0.07	0.01	0.10
Fe	2.75		2.36	2.06		1.04	1.00	1.43	0.86
Mg	1.48		1.59	1.64		1.06	0.98	0.29	0.96
Σoct.	5.78		5.50	5.39		2.86	2.80	2.54	2.63
Ca	0.00		0.11	0.13		0.09	0.08	0.15	0.03
Na	0.02		0.13	0.02		0.18	0.29	0.45	0.16
K	0.04		0.08	0.12		0.35	0.27	0.11	0.71
O	14		14	14		11	11	11	11

Symbols: Chl: chlorite, ML: mixed layer phases, Vrm: vermiculite, Na-Bt: sodian biotite, Bt: biotite. N.S.: not shown in the figures.

Bt–Vrm mixed-layers and to vermiculite has been documented by several authors (*e.g.*, Banfield & Eggleton 1988, Pozzuoli *et al*. 1992). On the other hand, phases with optical properties and textural features like the vermiculite described here have been interpreted to form from retrogression (or weathering) of biotite in the Malborough Schist (New Zealand) by Mortimer & Little (1998). These authors do not present, however, any definitive proof for this process. On the contrary, in other classical Paleozoic basements, vermiculite was interpreted as a prograde phase [see Velde (1978) and references therein], although detailed TEM–AEM studies are lacking.

In our case, TEM images indicate a complete transition between regular 1:1 Chl–Vrm mixed-layers and vermiculite, through intermediate phases with increasing proportions of vermiculite layers interstratified with chlorite (Fig. 8), suggesting that vermiculite formation represents a more advanced step in the chlorite transformation.

Nevertheless, secondary vermiculite did form locally in our samples from the retrogression of garnet, as described by Ruiz Cruz (2003) in one of the schist samples cited in this work (N–5). In this case, both structural and chemical differences permit a distinction between the two populations of vermiculite. A first generation of vermiculite grains parallel to the main schistosity consists of Chl–Vrm mixed-layers, characterized by Fe/(Fe + Mg) values less than 0.40. On the contrary, secondary vermiculite, which appears as a pseudomorph after garnet, consists of submicroscopic intergrowths of a variety of phases (muscovite, chlorite, vermiculite and smectite), the vermiculite showing Fe/(Fe + Mg) values of the order of 0.55. Although the possibility that vermiculite grains parallel to the schistosity represent retrogression of earlier biotite cannot be discarded on the basis of the textural relations, this possibility seems unlikely, as in higher-grade rocks (*e.g.*, N–6), biotite does not show signs of retrogression to vermiculite. On the contrary, as observed by TEM, local retrogression of vermiculite and biotite produces only kaolin-type minerals throughout the entire stratigraphic sequence.

Although it is evident from the XRD data that the names vermiculite and vermiculite-bearing mixed-layers accurately represent the actual thermal behavior of the phases described here, the phases formed during the metamorphic episode can hardly be considered to be vermiculitic. Chemical data as well as XRD patterns obtained after dehydration (see Figs. 3, 4) suggest that the vermiculite layers have a biotite-like structure with an incomplete interlayer cation occupancy, which favors their hydration (*i.e.,* to vermiculite) at surface conditions. Thus the sequence described here would probably correspond to a set of interstratified structures containing increasing proportions of mica layers. In summary, the entire set of vermiculitic phases described here probably represents metastable, intermediate structures between chlorite and biotite. Nevertheless, in our opinion, new experimental studies of the chlorite → biotite transformation, as well as detailed TEM–AEM studies of samples from the transition from the chlorite to the biotite zones in classic metamorphic basements, including some in which "metamorphic vermiculite" was initially described, would be necessary in order to unequivocally establish the status of these phases.

Chemical compositions as well as textural relations suggest that prograde vermiculitic phases form at the expense of chlorite, with a contribution from Al- and alkali-rich phases such as phengite, K-feldspar, and albite. Indeed, Na-bearing biotite appears to develop, in sample N–6, only in contact with albite grains (Ruiz Cruz 2004).

Although more than one mechanisms can operate during replacement of chlorite, TEM images show widespread transitions from one 14 Å layer to one 10 Å layer, suggesting a topotactic replacement (Giorgetti *et al*. 1997). This reaction, which has been described in both prograde and weathering processes (*e.g.,* Herbillon & Makumbi 1975, Veblen & Ferry 1983, Ahn *et al*. 1988, Murakami *et al*. 1996), is accompanied by significant chemical changes and a decrease in volume. TEM images indicate the loss of a brucite-like layer, which is replaced by interlayer cations. Chemical changes include, as a consequence, loss of divalent cations (Mg, Fe^{2+} and Mn^{2+}) and gain of K, Na, and Si. The topotactic replacement, which mainly occurs along the basal planes, was probably favored by the presence of fluids, at high $f(O_2)$ conditions, as the experimental conversion of chlorite to vermiculite requires partial oxidation of Fe^{2+} (Ross & Kodama 1976). Nevertheless, this reaction is not simple. Rather than a single step, it is evident that a sequence of structurally ordered and disordered states is involved in this reaction. Indeed, the ordered 2:1 and 1:1 structures and vermiculite certainly must be intermediate phases representing free-energy minima along the path of the reaction.

Estimation of the P–T conditions of the metamorphic assemblage

In addition to textural data, which point to overall equilibrium among the several metamorphic phases, the distribution of elements between coexisting phases has been used to test for equilibrium within metamorphic assemblages. In samples N–4, N–5 and N–6, we have calculated the distribution constants (K_D values) for the Fe^{2+}–Mg exchange between muscovite and vermiculite, muscovite and garnet, and vermiculite and garnet. The values obtained for pairs observed in contact have been summarized in Table 4. These data show that the distribution is coherent, indicating systematic partitioning, and suggesting a close approach to chemical equilibrium.

An estimation of the highest temperature of stability of the vermiculitic phases in samples N–4, N–5 and

N–6 is based on the calculation of the P–T conditions of formation of the coexisting minerals, given the lack of thermodynamic data for vermiculite. Calculations of the P–T conditions was carried out for samples N–5 and N–6 through the average PT method (Powell & Holland 1994), using the program THERMOCALC (Powell & Holland 1988), with the internally consistent thermodynamic dataset of Holland & Powell (1990). End-member activities were calculated using the computer program AX and the default values suggested by Powell & Holland (1988).

For sample N–5, we used the assemblage muscovite + chlorite + garnet + andalusite + quartz + H_2O. On the basis of this assemblage, there are insufficient reactions among the different end-members to calculate P and T simultaneously (Table 5), but the temperature interval obtained for pressures between 2 and 8 kbar is narrow (535 ± 30°C) (Fig. 9, reaction 2). In addition, assuming a mean temperature of 500°C, and a Si content in the white mica of 3.1 *apfu*, a minimum pressure of 3–4 kbar can be deduced from the geobarometer of Massone & Schreyer (1987) (Fig. 9, reaction 1).

For sample N–6, we used the paragenesis muscovite + biotite + garnet + andalusite + quartz + H_2O. With this

association, the P–T conditions deduced with THERMOCALC were: 500 ± 50°C (Table 5, Fig. 9, reaction 4) and 5 ± 1.5 kbar (Table 5, Fig. 10, reaction 3).

Finally, in sample N–4, the lack of andalusite prevents an estimate of P and T with THERMOCALC. Nevertheless, the garnet–muscovite geothermometer, with various calibrations (Krogh & Råheim 1978, Hynes & Forest 1988) and several garnet solid-solution models (ideal mixing: Hodges & Spear 1982, Ganguly & Saxena 1984, Hoinkes 1986), gives temperatures ranging from 400 to 475°C.

Correlation between the vermiculite structure and temperature of formation

The schist samples used for the P–T estimates in this work (N–4, N–5 and N–6) correspond to the highest metamorphic grade observed in the Maláguide complex and the passage to the underlying Benamocarra unit. Previous investigators of P–T conditions in the Maláguide greywackes and phyllites (Silurian to Carboniferous) relied on several chlorite geothermometers and the geobarometer of Massone & Schreyer (1987) (Ruiz Cruz 1999, 2001, Ruiz Cruz & Rodríguez Jiménez 2002). These data (Table 6) show a clear relation between structural characteristics of vermiculitic phases and mineral paragenesis, mainly with chlorite content and the presence of other metamorphic phases (*e.g.*, chloritoid, paragonite, garnet). The four groups of samples defined in the Introduction section are characterized by the following features:

(1) Chlorite-rich samples contain random to ordered 1:2 Mi–Chl mixed-layer phases. In these samples, chlorite is easily detected by XRD, as its basal reflections do no overlap those of the mixed-layer phases (Fig. 3B).

(2) Chlorite-poor samples without garnet mainly contain ordered 1:1 Chl–Vrm mixed-layer phases, and

TABLE 4. DISTRIBUTION CONSTANTS FOR EXCHANGE REACTIONS BETWEEN PAIRS OF ANALYZED MINERALS

Sample	K_D Ms–Vrm	K_D Ms–Grt	K_D Vrm–Grt
N-4	0.66; 0.55; 0.56	0.065; 0.078	0.12; 0.09; 0.15; 0.12; 0.14; 0.11
N-5	0.53; 0.48; 0.52	0.066; 0.076	0.18; 0.19; 0.21
N-6	0.75; 0.67; 0.71; 0.74	0.062; 0.053	0.070; 0.075

Symbols: Ms: muscovite, Bt: biotite, Vrm: vermiculite, Grt: garnet.

TABLE 5. ESTIMATE OF P–T CONDITIONS FOR SAMPLES N-5 AND N-6

N-5	Set of reactions (average temperature)									
	Ctn + Ams + 4 Qtz = 3 Prp + 8 H_2O	P	2.0	3.0	4.0	5.0	6.0	7.0	8.0	
	3 Ams + 8 Qtz = 4 Prp + 2 And + 12 H_2O	ave. T	530	536	539	539	538	535	532	
	3 "Daph" + 3 Ams + 12 Qtz = 4 Prp + 5 Alm + 24 H_2O	s.d.	26	27	28	30	31	32	33	
	Cel + 2 Ams + 4 Qtz = Ms + 3 Prp + 8 H_2O									
N-6	Set of reactions (average temperature)	P		2.0	3.0	4.0	5.0	6.0	7.0	8.0
	2 Pg + Grs + 3 Qtz = 3 An + 2 Ab + 2 H_2O	avT		401	458	481	506	533	561	588
	4 Pg + 3 Cel + Grs = 2 Ms + 3 An + 4 Ab + Eas + 4 H_2O	s.d.		82	70	55	52	46	40	34
	4 Pg + 2 Cel + Grs = Ms + 3 An +4 Ab + Eas + 4 H_2O									
	4 Pg + 2 Cel + 2 Grs + Alm = 6 An + 4 Ab + Ann + Eas + 4 H_2O									

	Set of reactions (average pressure)	T	300	350	400	450	500	550	600	650	700
	Ann + 3 Eas + 6 Qtz = 2 Ms + Alm + 2 Phl	ave. P	3.0	3.6	4.1	4.6	5.1	5.6	6.0	6.5	6.9
	6 Phl + 5 Ann + 12 And = 4 Cel + 5 Alm + 7 Eas	s.d.	1.04	1.11	1.19	1.27	1.34	1.42	1.49	1.57	1.64

Symbols: Ab: albite, Alm: almandine, Ams: amesite, An: anorthite, And: andalusite, Ann: annite, Cel: celadonite, Ctn: clintonite, "Daph": "daphnite", Eas: eastonite, Grs: grossular, Ms: muscovite, Pg: paragonite, Phl: phlogopite, Prp: pyrope, Qtz: quartz.
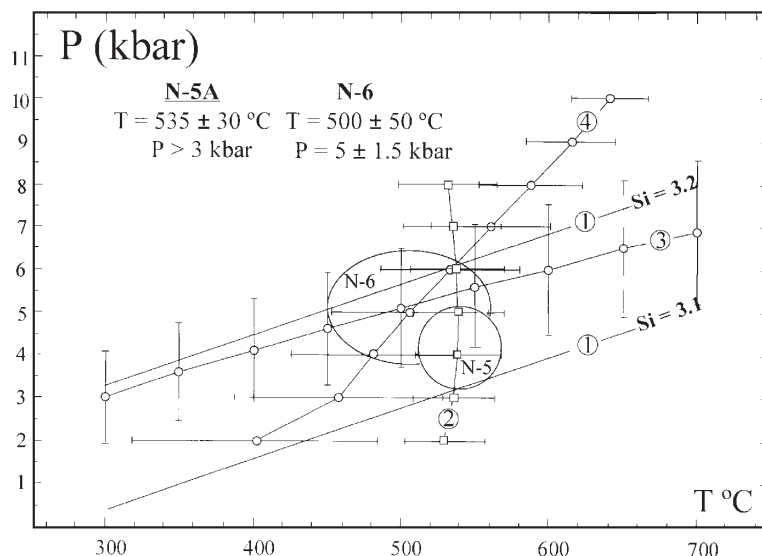
FIG. 9. P–T diagram showing the estimated field of stability of samples N–5 and N–6. Reactions plotted in the figure were calculated using THERMOCALC (Powell & Holland 1988), except for reaction 1, which is based on Si content of white mica (Massone & Schreyer 1987).

TABLE 6. COMPILATION OF P-T ESTIMATES

Group	Sample	Mineral assemblage*	T (°C)	P (kbar)	Ref
I	PZ-7	Chl + 1:2 Mi-Chl + Ms + Kln	125-250 (1)	3 ± 1 (5)	1
	PZ-8	Chl + Ms	125-250 (1)	3 ± 1 (5)	1
II	CH-4	Chl + regular 1:1 Chl-Vrm + Ms	300 ± 30 (1)	3.5 ± 1 (5)	2
	CH-121	Chl + regular 1:1 Chl-Vrm + Ms + Cld	350 ± 20 (1)	4 ± 1 (5)	3
	PZ-19	(Chl) + regular 1:1 Chl-Vrm + Ms	300 ± 30 (1)	3.5 ± 1 (5)	2
III	N-4	(Chl) + Vrm + Ms + Grt	400-475 (2)	4 ± 1 (5)	4
	N-5	(Chl) + Vrm-rich Chl-Vrm + Vrm + Ms + Grt + And	535 ± 30 (3)	3-4 (3)	4
IV	CH-8	Vrm + (Vrm-rich Chl-Vrm) + Bt + Ms + Pg	>400°C (4)	4 ± 1 (5)	2
	N-6	Na-Bt + Bt + Grt + And	500 ± 50 (3)	5 ± 1 (3)	4

Symbols: ML: mixed-layer phases, Chl: chlorite, Ms: muscovite, Pg: paragonite, Bt: biotite, Vrm: vermiculite, Mi-Chl: mica–chlorite mixed-layer phases, Chl–Vrm: chlorite–vermiculite mixed-layer phases, Kln: kaolin mineral, Cld: chloritoid, And: andalusite, Grt: garnet, Na-Bt: sodian biotite.
* Excluding quartz, feldspar, carbonate and Fe oxides.
Notes: (1): Chlorite geothermometer (Hillier & Velde 1991), (2) Garnet–muscovite geothermometer (Krogh & Raheim 1978, Hynes & Forest 1988), (3) THERMOCALC (Powell & Holland 1994), (4) Yardley (1989), (5) Phengite geobarometer (Massone & Schreyer 1987).
References: 1: Ruiz Cruz (2001), 2: Ruiz Cruz (1999), 3: Ruiz Cruz & Rodriguez Jiménez (2002), 4: this work.

subordinate 1:2 mica–chlorite mixed-layer phases. In these samples, chlorite is only occasionally detected by XRD.

(3) Chlorite-poor samples containing garnet are characterized by the presence of dominant grains of vermiculite. Relict grains of unaltered chlorite are only rarely observed by optical microscopy. Vermiculitic grains consist either of randomly ordered Chl–Vrm with a chlorite–vermiculite ratio of less than 2 or of true vermiculite.

(4) Biotite-bearing samples contain true biotite and Na-rich hydrated biotite (or vermiculite). TEM–AEM observation of these samples also indicate the lack of discrete packets of chlorite.

The structural evolution of vermiculitic phases, related to tectonic depth, is thus characterized by decreasing Chl content in the mixed-layered structures, coupled with a decrease in chlorite in the mineral assemblages, in such a way that chlorite coexists with vermiculitic phases, but it is lacking in biotite-bearing samples. A complete sequence of transformation of chlorite to biotite through well-defined intermediate structures has not been previously described, and is similar to the smectite-to-illite and the smectite-to-chlorite transformations (*e.g.* Nadeau *et al.* 1985, Bettison & Schiffman 1988: Schiffman & Fridleifsson 1991, Pollastro 1993, Huang *et al.* 1993).

CONCLUDING REMARKS

Chemical data obtained by electron-probe micro-analysis and electron microscopy indicate that the compositional field of vermiculitic phases spans the chlorite and biotite fields, with several well-defined

structural organizations, characterized by a decrease of the chlorite component. The chemical evolution includes an increase in Si and Na + K. Most phases described are probably metastable, with the ordered 2:1 and 1:1 structures and vermiculite representing free-energy minima along the path of the reaction. Nevertheless, more experimental studies are necessary to unambiguously define the status of vermiculite. The accurate determination of these structures can only be made by TEM, but the XRD study supplies a correct approach.

P–T estimates reveal that the stability field of "metamorphic vermiculite" overlaps that of chlorite and extends to the biotite field, at ~500°C. Nevertheless, vermiculitic layers must be considered as biotite layers with a low charge, that rapidly rehydrate under meteoric conditions.

REFERENCES

ABAD, I., NIETO, F., PEACOR, D.R. & VELILLA, N. (2003): Prograde and retrograde diagenetic and metamorphic evolution in metapelitic rocks of Sierra Espuña (Spain). *Clay Minerals* **38**, 1-23.

AHN, JUNG-HO, PEACOR, D.R. & COOMBS, D.S. (1988): Formation mechanisms of illite, chlorite and mixed-layers illite/chlorite in Triassic volcanogenic sediments from the Southland Syncline, New Zealand. *Contrib. Mineral. Petrol.* **99**, 82-89.

AZAÑÓN, J.M. (1994): *Metamorfismo de alta presión/baja temperatura, baja presión/alta temperatura y tectónica del Complejo Alpujárride (cordilleras Bético-Rifeñas)*. Tesis. Universidad de Granada, Granada, Spain.

AZAÑÓN, J.M. & CRESPO BLANCO, A. (2000): Exhumation during a continental collision inferred from the tectono-metamorphic evolution of the Alpujárride complex in the central Betics (Alboran Domain, SE Spain). *Tectonics* **19**, 549-565.

BANFIELD, J.F. & EGGLETON, R.A. (1988): Transmission electron microscope study of biotite weathering. *Clays Clay Minerals* **36**, 47-60.

BANFIELD, J.F. & MURAKAMI, T. (1998): Atomic-resolution transmission electron microscope evidence for the mechanism by which chlorite weathers to 1:1 semi-regular chlorite–vermiculite. *Am. Mineral.* **83**, 348-357.

BETTISON, L.A. & SCHIFFMAN, P. (1988): Compositional and structural variation of phyllosilicates from the Point Sal Ophiolite, California. *Am. Mineral.* **73**, 62-76.

BLACK, P.M. (1975): Mineralogy of New Caledonian metamorphic rocks. IV. Sheet silicates from Ouégoa district. *Contrib. Mineral. Petrol.* **49**, 269-284.

BROWN, E.H. (1967): The greenschist facies in part of eastern Otago, New Zealand. *Contrib. Mineral. Petrol.* **14**, 259-292.

DEMPSTER, T.J. & JACKSON, R.A. (1996): Na-biotite in Dalradian pelitic schists, Angus. *Scot. J. Geol.* **32**, 173-177.

FRANCESCELLI, M., MELLINI, M., MEMMI, I. & RICCI, C.A. (1986): Fine-scale chlorite–muscovite association in low-grade metapelites from Nurra (NW Sardinia), and the possible misidentification of metamorphic vermiculite. *Contrib. Mineral. Petrol.* **93**, 137-143.

GANGULY, J. & SAXENA, S.K. (1984): Mixing properties of aluminosilicate garnets: constraints from natural and experimental data, and applications to geothermobarometry. *Am. Mineral.* **69**, 88-97.

GIORGETTI, G., MEMMI, I. & NIETO, F. (1997): Microstructures of intergrown phyllosilicate grains from Verrucano metasediments (northern Apennines, Italy). *Contrib. Mineral. Petrol.* **128**, 127-138.

HERBILLON, A.J. & MAKUMBI, M.N. (1975): Weathering of chlorite in a soil derived from a chloritoschist under humid tropical conditions. *Geoderma* **13**, 89-104.

HILLIER, S. & VELDE, B. (1991): Octahedral occupancy and the chemical composition of diagenetic (low-temperature) chlorite. *Clay Minerals* **26**, 149-168.

HODGES, K.V. & SPEAR, F.S. (1982): Geothermometry, geobarometry and the Al_2SiO_5 triple point at Mt. Moosilauke, New Hampshire. *Am. Mineral.* **67**, 1118-1134.

HOINKES, G. (1986): Effect of grossular-content in garnet on the partitioning of Fe and Mg between garnet and biotite. *Contrib. Mineral. Petrol.* **92**, 393-399.

HOLLAND, T.J.B. & POWELL, R. (1990): An enlarged and updated internally consistent thermodynamic dataset with uncertainties and correlations: the system $K_2O–Na_2O–CaO–MgO–MnO–FeO–Fe_2O_3–Al_2O_3–TiO_2–SiO_2–C–H_2–O_2$. *J. Metam. Geol.* **8**, 89-124.

HUANG, WUU-LIANG, LONGO, J.M. & PEVEAR, D.R. (1993): An experimentally derived kinetic model for smectite-to-illite conversion and its use as geothermometer. *Clays Clay Minerals* **41**, 162-177.

HYNES, A. & FOREST, R.C. (1988): Empirical garnet–muscovite geothermometry in low-grade metapelites, Selwyn Range (Canadian Rockies). *J. Metam. Geol.* **6**, 297-309.

JOHNSON, L.J. (1964): Occurrence of regularly interstratified chlorite–vermiculite as a weathering product of chlorite in a soil. *Am. Mineral.* **49**, 556-572.

KERRICK, D.M. & COTTON, W.R. (1971): Stability reactions of jadeite pyroxene in Franciscan metagreywackes near San José, California. *Am. J. Sci.* **271**, 350-369.

KROGH, E.J. & RÅHEIM, A. (1978): Temperature and pressure dependence of Fe–Mg partitioning between garnet and phengite, with particular reference to eclogites. *Contrib. Mineral. Petrol.* **66**, 75-80.

LEE, J.H. & PEACOR, D.R. (1985): Ordered 1:1 interstratification of illite and chlorite: a transmission and analytical electron microscopy study. *Clays Clay Minerals* **33**, 463-467.

LORIMER, G.W. & CLIFF, G. (1976): Analytical electron microscopy of minerals. *In* Electron Microscopy in Mineralogy (H.R. Wenk, ed.). Springer-Verlag, New York, N.Y. (506-519).

MÄKEL, G.H. (1985): The geology of the Maláguide Complex and its bearing on the geodynamic evolution of the Betic-Rif orogen (southern Spain and northern Morocco). *GUA Papers of Geol.* **22**.

MARESCH, W.V., MASSONE, H.-J. & CZANK, M. (1985): Ordered and disordered chlorite/biotite interstratifications as alteration products of chlorite. *Neues Jahrb. Mineral. Abh.,* **152**, 79-100.

MASSONE, H.-J. & SCHREYER, W. (1987): Phengite geobarometry based on the limiting assemblage with K-feldspar, phlogopite, and quartz. *Contrib. Mineral. Petrol.* **96**, 212-224.

MELLINI, M., NIETO, F., ALVAREZ, F. & GÓMEZ-PUGNAIRE, M.T. (1991): Mica–chlorite intermixing and altered chlorite from the Nevado–Filábride micaschists, southern Spain. *Eur. J. Mineral.* **3**, 27-38.

MIYASHIRO, A. (1994): *Metamorphic Petrology*. UCL Press, London, U.K.

MORTIMER, N. & LITTLE, T. (1998): Altered biotites in the Marlborough Schist, New Zealand? *N.Z. J. Geol. Geophys.* **41**, 105-109.

MURAKAMI, T., ISOBE, H., SATO, T. & OHNUKI, T. (1996): Weathering of chlorite in a quartz–chlorite schist. I. Mineralogical and chemical changes. *Clays Clay Minerals* **44**, 244-256.

NADEAU, P.H., WILSON, M.J., MCHARDY, W.S. & TAIT, J.M. (1985): The conversion of smectite to illite during diagenesis: evidence from some illitic clays from bentonites and sandstones. *Mineral. Mag.* **49**, 393-400.

NICOT, E. (1981): Les phyllosilicates des terrains précambriens du Nord–Ouest du Montana (USA) dans la transition anchizone – épizone. *Bull. Minéral.* **104**, 615-624.

POLLASTRO, R.M. (1993): Considerations and applications of the illite/smectite geothermometer in hydrocarbon-bearing rocks of Miocene to Mississippian age. *Clays Clay Minerals* **41**, 119-133.

POWELL, R. & HOLLAND, T.J.B. (1988): An internally consistent data set with uncertainties and correlations. 3. Applications to geobarometry, methods, worked examples and a computer program. *J. Metam. Geol.* **6**, 173-204.

POWELL, R. & HOLLAND, T.J.B. (1994): Optimal geothermometry and geobarometry. *Am. Mineral.* **79**, 120-133.

POZZUOLI, A., VILA, E., FRANCO, E., RUIZ-AMIL, A. & DE LA CALLE, C. (1992): Weathering of biotite to vermiculite in quaternary lahars from Monti Ernici, central Italy. *Clay Minerals* **27**, 175-184.

PROUST, D. (1982): Supergene alteration of metamorphic chlorite in an amphibolite from Massif Central, France. *Clay Minerals* **17**, 159-173.

PROUST, D., EYMERY, J.P. & BEAUFORT, D. (1986): Supergene vermiculitization of a magnesian chlorite: iron and magnesium removal process. *Clays Clay Minerals* **34**, 572-580.

PUGA, E., DÍAZ DE FEDERICO, A. & NIETO, J.M. (2002): Tectonostratigraphic subdivisión and petrological characterisation of the deepest complexes of the Betic zone: a review. *Geodin. Acta* **15**, 23-43.

ROSS, G.L. (1975): Experimental alteration of chlorite into vermiculite by chemical oxidation. *Nature* **255**, 133-134.

ROSS, G.J. & KODAMA, H. (1976): Experimental alteration of chlorite into a regularly interstratified chlorite–vermiculite by chemical oxidation. *Clays Clay Minerals* **24**, 183-190.

ROSS, G.J., WANG, C., OZKEN, A.I. & REEA, H.W. (1982): Weathering of chlorite and mica in a New Brunswick podzol developed on till derived from chlorite–mica schist. *Geoderma* **27**, 255-267.

RUIZ CRUZ, M.D. (1999): New data for metamorphic vermiculite. *Eur. J. Mineral.* **11**, 533-548.

RUIZ CRUZ, M.D. (2001): Mixed-layer mica–chlorite in very low-grade metaclastites from the Maláguide Complex (Betic Cordilleras, Spain). *Clay Minerals* **36**, 307-324.

RUIZ CRUZ, M.D. (2003): Two stages of "metamorphic vermiculite" growth in schists from the Maláguide Complex (Betic Cordillera, Spain*). Can. Mineral.* **41**, 1397-1412.

RUIZ CRUZ, M.D. (2004): Sodium- and intermediate sodium–potassium biotite in schists from the Betic Cordillera (Spain). *Clays Clay Minerals* **52**, 603-612.

RUIZ CRUZ, M.D. & RODRÍGUEZ JIMÉNEZ, P. (2002): Correlation between crystallochemical parameters of phyllosilicates and mineral facies in very low-grade metasediments of the Betic Cordillera (Spain): a synthesis. *Clay Minerals* **37**, 169-185.

RUIZ CRUZ, M.D. & NOVAK, J. (2003): Metamorphic chlorite and "vermiculitic" phases in mafic dikes from the Maláguide Complex (Betic Cordillera, Spain). *Eur. J. Mineral.* **15**, 67-80.

SCHIFFMAN, P. & FRIDLEIFFSON, G.O. (1991): The smectite to chlorite transition in drillhole NJ–15, Nesjavellir Geothermal Field, Iceland: XRD; BSE and electron microprobe investigations. *J. Metam. Geol.* **9**, 679-696.

SANZ DE GALDEANO, C. & ALFARO, P. (2004): Tectonic significance of the present relief of the Betic Cordillera. *Geomorphology* **63**, 178-190.

SCHREYER, W., ABRAHAM, K. & KULKE, H. (1980): Natural sodium phlogopite coexisting with potassium phlogopite and sodian aluminian talc in a metamorphic evaporite sequence from Derrag, Tell Atlas, Algeria. *Contrib. Mineral. Petrol.* **74**, 223-233.

SPEAR, F.S., HAZEN, R.M. & RUMBLE, D. (1981): Wonesite; a new rock-forming silicate from the Post Pond Volcanics, Vermont. *Am. Mineral.* **66**, 100-105.

VEBLEN, D.R. & FERRY, J.M. (1983): A TEM study of the biotite–chlorite reaction and comparison with petrologic observations. *Am. Mineral.* **68**, 1160-1168.

VELDE, B. (1978): High temperature or metamorphic vermiculites. *Contrib. Mineral. Petrol.* **66**, 319-323.

YARDLEY, B.W.D. (1989): *An Introduction to Metamorphic Petrology*. Longman, Harlow, U.K.